HHS Public Access

Author manuscript

J Mass Spectrom. Author manuscript; available in PMC 2018 November 01.

Published in final edited form as:

J Mass Spectrom. 2017 November ; 52(11): 720–727. doi:10.1002/jms.3975.

Infrared ion spectroscopy inside a mass-selective cryogenic 2D linear ion trap

Adam P. Cismesia, **Larry F. Tesler**, **Matthew R. Bell**, **Laura S. Bailey**, and **Nicolas C. Polfer***

Abstract

We demonstrate operation of the first cryogenic 2D linear ion trap (LIT) with mass-selective capabilities. This trap presents a number of advantages for infrared ion "action" spectroscopy studies, particularly those employing the "tagging/messenger" spectroscopy approach. The high trapping efficiencies, trapping capacities, and low detection limits make 2D LITs a highly suitable choice for low-concentration analytes from scarce biological samples. In our trap, ions can be cooled down to cryogenic temperatures to achieve higher-resolution infrared spectra, and individual ions can be mass selected prior to irradiation for a background-free photodissociation scheme. Conveniently, multiple tagged analyte ions can be mass isolated and efficiently irradiated in the same experiment, allowing their infrared spectra to be recorded in parallel. This multiplexed approach is critical in terms of increasing the duty cycle of infrared ion spectroscopy, which is currently a key weakness of the technique. The compact design of this instrument, coupled with powerful mass selection capabilities, set the stage for making cryogenic infrared ion spectroscopy viable as a bioanalytical tool in small molecule identification.

Keywords

vibrational spectroscopy; tagging; lasers; ion spectroscopy; linear ion trap; cryogenic

Introduction

Infrared (IR) ion spectroscopy combines the sensitivity and separation capabilities of mass spectrometry with the high structural information from vibrational spectroscopy. The specific information on a wide range of chemical moieties (based on diagnostic vibrations) makes infrared ion spectroscopy stand out among the structural mass spectrometry techniques. For small molecule identification (e.g. metabolites, illicit drugs), where spectral congestion is limited, the technique presents a potential "game changer". Yet, despite this potential, key challenges remain to make infrared ion spectroscopy a routine bioanalytical technique.[1]

The currently most popular infrared ion action spectroscopy approach, infrared multiple photon dissociation (IRMPD) spectroscopy,[2, 3] has some shortcomings that are in fact related to the multiple-photon absorption scheme. Multiple-photon absorption leads to band

*Correspondence to Nicolas C. Polfer, Department of Chemistry, University of Florida, P.O. Box 117200, Gainesville, FL 32611-7200, USA. polfer@chem.ufl.edu.

broadening and redshifts (i.e., shifts to lower frequencies), which may obfuscate inherent, more subtle differences in the absorptions of closely-related ions and structures. This also leads to distortions in the relative band intensities, making a comparison to computed IR spectra more challenging. Finally, multiple-photon absorption requires intense tunable light sources, which constrains its spectral range to the hydrogen stretching region for benchtop light sources (2500–4000 cm^{-1}). Measurements in the important fingerprint region (500–2000 cm^{-1}) require free electron lasers housed at user facilities (FELIX,[4] CLIO,[5] FHI[6]).

Infrared ion spectroscopy carried out at cryogenic temperatures overcomes some of these challenges. In infrared predissociation spectroscopy, [7–11] which is also referred to as vibrational predissociation spectroscopy,[8] "messenger"[7] or "tagging"[12] spectroscopy, an ion of interest forms a non-covalent complex with a weakly-bound atom or molecule, a "tag", such as H_2,[8] Ne or N_2. [13] Upon resonant absorption of a single photon, this weakly-bound tag is detached, changing the mass back to the bare mass of the ion. Critically, this means that the action spectroscopy approach reverts to a single-photon and thus linear spectroscopy regime. Additionally, the bands in cryogenic infrared ion spectra are generally narrower than the corresponding IRMPD spectra, due to a combination of factors. There are of course drawbacks to this method, including perturbation from the tag which may affect the IR spectrum, as well as reduced ion signal due to low tagging efficiencies.

A solvent-adducted complex presents another form of a tagged analyte ion. IR spectroscopic studies on hydrated clusters allow elucidation of solvation processes,[14, 15] and are therefore of great interest in fundamental studies. However, their rich OH stretch modes are a complicating factor for more analytical applications, where the purpose of the tag is mainly to facilitate photodissociation. The solvent molecule acetonitrile (ACN) considered here does not exhibit hydrogen stretching modes that would overlap with diagnostic OH and NH stretching modes. The strong dipole of ACN, however, leads to a stronger interaction energy than H_2 or N_2, thus potentially requiring absorption of more than one photon to induce photodissociation. We will therefore employ the more generic term infrared photodissociation (IRPD) to denote dissociation of these solvent-tagged analytes.

Designs of cryogenic ion traps are another area that requires further developments, in order to make the technique compatible with the high sensitivity requirements of biological samples. Cryogenic trap designs thus far have emphasized the capabilities of these traps to cool ions down to very low temperatures.[8, 10, 13, 16–21] Tagged ions are then generally moved to other mass analyzers, such as a time-of-flight drift[8–10] tube for mass-selective manipulation. A few studies have demonstrated mass-selective cryogenic Fourier transform ion cyclotron resonance (FTICR) traps,[15, 18, 22] but no mass-selective 2D RF ion traps have been reported to date. Here, we report cryogenic infrared spectroscopy inside a mass-selective 2D linear ion trap. Ions are cooled to cryogenic temperatures, mass isolated, irradiated, and mass detected in the same device. The advantages of this design with respect to operation, sensitivity, duty cycle, and other experimental considerations are discussed.

Experimental

Mass spectrometry

A custom mass spectrometer employed in a series of IRMPD studies has been described in detail elsewhere.[23] Briefly, the instrument consists of a commercial electrospray ionization (ESI) source (Analytica of Branford, Branford, CT) fitted with a custom ion funnel.[24] The ions are then bent 90° by an ion deflector into a quadrupole mass filter (QMF) (Ardara Technologies, Monroeville, PA) for mass selection. A second ion deflector allows either detection of ions on a conversion dynode electron multiplier, or, if bent the other way, movement of the ions to a 3D quadrupole ion trap (QIT) (Jordan ToF Products, Grass Valley, CA). Here, the compact ion cloud is subjected to intense radiation from a tunable optical parametric oscillator/amplifier (OPO/A), followed by ejection of the photofragment ions and remaining precursor ions into the drift tube of a time-of-flight (TOF) mass analyzer (Jordan TOF Products, Grass Valley, CA).

This instrument has now been updated with an extension to allow cryogenic infrared ion spectroscopy studies. This extension is positioned off the “empty” port on the second deflector. It consists of an accumulation trap, Einzel and steering lenses, as well as a cryogenic 2D linear ion trap, which is mounted from a closed cycle helium cryostat. Figure 1 depicts a cross-sectional view of this custom cryogenic 2D linear ion trap, named *cryoLIT* for the purpose of this paper. The *cryoLIT* is composed of planar RF electrodes for radial trapping, and DC electrodes for axial trapping, and thus has some similarities in design to previously published works on non-cryogenic 2D LITs.[25, 26] All electrodes are made of stainless steel, and custom sapphire spacers are employed to allow heat conduction between the electrodes and the cryostat cold finger. Sapphire is commonly employed in cryogenic traps, due to its high thermal conductivity at cryogenic temperatures, while also being a suitable electrical insulator. A heat shield (not shown) is placed around the *cryoLIT* to minimize black-body radiation of the electrodes and ions.

The *cryoLIT* is driven by a commercial Velos RF power supply (Thermo-Fisher, San Jose, CA) operated at a drive frequency of 1.108 MHz. Trapping of externally injected ions is facilitated by a helium gas pulse using a solenoid pulsed valve (Parker Series 99, Hollis, NH). This gas pulse also serves the purpose of collisionally cooling ions down to cryogenic temperatures. After a pump-down delay (200–480 ms), ions of interest are mass isolated via dipolar excitation on the left/right RF electrodes with a stored waveform inverse Fourier transform (SWIFT).[27] followed by irradiation from the tunable output from the OPO/A, and finally mass detection via an instability scan. By applying a dipolar waveform (at 369 kHz) on the left/right RF electrodes, ions are selectively ejected through slits in those two electrodes to be directed to a conversion dynode/electron multiplier detector. Currently, these experiments were conducted at a speed of one spectrum per second, however, by reducing the pumpdown delay it is possible to perform these experiments considerably faster. Timings of voltages in the experiments are under the control of TTL pulses, delay generators and microcontrollers (Teensy LC, Sherwood, OR), to ensure that the experimental sequence is in sync with the OPO/A output. Data acquisition is handled by a custom LabView program. A

more detailed description of this instrument, including its operation, will be the subject of a forthcoming publication.[28]

Para-aminobenzoic acid (PABA) and tyramine (4-hydroxyphenethylamine) come from commercial vendors (Sigma Aldrich, St. Louis, MO), and are used without further purification. ESI solutions consist of analyte concentrations down to 10^{-7} M in acetonitrile (ACN), with 1% (vol) formic acid added to assist ionization in positive ion mode. ESI source conditions and ion transfer optics are optimized to generate abundant ion signal of the solvent-tagged analyte ions, denoted as M●ACN. Total sample consumption for a complete IR spectrum can be estimated at 60 μmol, based on infusion rates of 2μL/min for ~300 min.

Infrared spectroscopy

The tunable OPO/A (LaserVision, Bellevue, WA) is pumped by a Surelite III unseeded 1064 nm Nd:YAG laser (Continuum, San Jose, CA) producing a pump photon λ_{pump}. A detailed description of this OPO/A setup has been given previously,[29] and thus here we will only focus on aspects prescient to wavelength calibration and power normalization. The OPO/A output wavelength, $\lambda_{OPO/A}$, is generated in a difference-frequency process described by the following energy conservation equation:

$$\frac{1}{\lambda_{OPO/A}} = \frac{1}{\lambda_1} - \frac{1}{\lambda_{pump}} \quad \text{Eq 1}$$

where λ_1 is generated in the first non-linear crystal, and is tunable from 700–920 nm. By measuring λ_1 and, in our case, the doubled pump photon at 532 nm, $\lambda_{pump}/2$, with appropriate wavemeters (HR2000+/4000, Ocean Optics, Dunedin, FL), a calibrated value of $\lambda_{OPO/A}$ can be derived. The central wavelength of the doubled pump is measured at 532.106 nm, which is equivalent to 18,793 cm^{-1} at a full-width half-maximum (FWHM) of ~2 cm^{-1}, compared to a FWHM of ~7 cm^{-1} for λ_1. The resolution of the wavemeters is 0.04–0.05 nm, which is equivalent to 0.7–1 cm^{-1}, and thus the central wavenumber of the OPO/A output can be established at an accuracy of ≤ 1.2 cm^{-1}. The OPO/A pulse energy is measured with energy meters suitable for various energy ranges (Models PE9-C and PE50BF-DIF-C, Ophir, North Logan, UT). For the IR beam alignments employed here, the cryogenic IRPD experiments made use of pulse energies up to 10 mJ, which compares to pulse energies up to 25 mJ for IRMPD spectroscopy. Note that in all photodissociation experiments the ions are irradiated with a single OPO/A pulse, even if in a trap, the ion cloud could be subjected to multiple pulses.

The photodissociation yields for an analyte molecule M that are employed in IRMPD and IRPD are given by the following equations:

$$yield_{IRMPD} = -ln\left[1 - \frac{\sum(photofragments)}{\sum(photofragments + M)}\right] \quad \text{Eq 2}$$

$$yield_{IRPD} = -ln\left[1 - \frac{M}{M + M\bullet ACN}\right] \quad \text{Eq 3}$$

Somewhat confusingly, the ion signal for M is a *precursor* ion for IRMPD, but a *photofragment* for IRPD. This reflects the different methodologies employed, as tagged ions are photodissociated to the bare ion in IRPD. In all cases, the yields are normalized for OPO/A output power.

Results and Discussion

Para-aminobenzoic acid

The protonation of para-aminobenzoic acid (PABA) presents an intriguing case for ion structure studies.[24, 30–32] When electrosprayed from protic solvents, the carboxylic acid group is the observed site of proton attachment. Conversely, when sprayed from the aprotic solvent acetonitrile, the amino group is found to be protonated. Figure 2 shows a series of mass spectra for the PABA experiments. The raw ESI mass spectrum in Figure 2A shows the abundant ACN adduct. It also shows a lesser abundance of the hydrated complex PABA●H_2O. This species was not considered here, due to its (likely) more congested IR spectrum. The PABA●ACN complex can be readily mass selected, without any trace of background dissociation to the bare PABA ion (2B). Upon resonant absorption, abundant photodissociation to bare PABA is observed (2C), demonstrating the action spectroscopy scheme. Note that the observation of PABA●ACN may in principle be due to incomplete desolvation, or alternatively and additionally, due to attachment of ambient ACN in the source.

An important factor to consider in tagging spectroscopy is the efficiency with which tagged ions can be generated. The efficiency with which a particular tagged state with *x* ACN molecules is generated, M●ACN_x is defined here as:

$$tagging\ efficiency\ for\ M \bullet ACN_x\ (\%) = \frac{M \bullet ACN_x}{\sum_{i=0}^{n} (M \bullet ACN_i)} \times 100 \quad \text{Eq 4}$$

where the relative abundance of a particular tagged ion M●ACN_x is divided by the summed abundances of all untagged (M●ACN_0 = M) and tagged (M●ACN_i) ions up to a maximum *n*.

The high single tagging efficiency for PABA (i.e., 53.4%) stands out, yet there is no evidence of doubly- or even more highly-tagged ions (2A). This means that the analyte ion signal is minimally diluted, resulting in enhanced sensitivity. This behavior stands in sharp contrast with cryogenic tagging approaches using for instance H_2, where single tagging efficiencies are rarely higher than a few percent, and where the signal can be distributed over multiple tagged species.[8]

Figure 3 contrasts the cryogenic (17K) IRPD spectrum for ACN-tagged PABA (3A) with a previously recorded IRMPD spectrum of bare PABA (3B),[24] both in the protonated form. It

should be noted that the actual temperature of the ions is not known in these experiments. Still, tagging experiments at 25K have shown that N_2 could be attached to the protonated tryptophan ions, and that a rough IRPD spectrum could be recorded in that way (see Supporting Information, Figure S1).

The vibrational mode assignment is based on a comparison to a computed IR spectrum for bare PABA, and this is summarized in Table 1. Carboxylic acid OH, amino NH_3^+ and aromatic CH stretches can be detected for the analyte. Based on gas-phase infrared absorption measurements, it known that ACN has a CH stretching mode at 2954 cm^{-1},[33] which is thus assigned to the tag. Not surprisingly, the bands in the IRMPD spectrum are slightly broader, and the band positions are redshifted (i.e., observed at lower frequencies) compared to the IRPD spectrum (by 15–40 cm^{-1}). Even more crucially, the IRMPD spectrum shows very limited evidence for the higher-frequency NH_3^+ stretching bands. All of these observations can be rationalized by the well-documented anharmonic effects associated with multiple-photon absorption. Each photon absorbed in IRMPD causes a redshift in the vibrational frequency, and thus the mode shifts out of resonance with the laser. If it were not for band broadening effects (due to a higher density of states at higher internal energies), molecules would not be able to absorb multiple photons from a monochromatic light source. Still, for some vibrational modes this redshift is pronounced enough to prevent the ion from reaching the dissociation threshold, and thus no photodissociation is observed.

For PABA●ACN, the relative IRPD band intensities for the NH and CH stretching bands are much suppressed compared to the OH stretching mode, in marked contrast to their relative computed IR intensities. This suggests that more than one IR photon needs to be absorbed to induce photodissocation, at least over some of this wavelength range. In other words, IRPD is also subject to anharmonic effects because of multiple-photon dissociation, as well as redshifting due to hydrogen bonding in the tagged complex. Nonetheless, all of the IRPD bands are observed at higher frequencies than the corresponding IRMPD bands. Even more importantly, the observation of a higher-frequency NH_3^+ band (which is not seen in IRMPD) and even low-intensity CH stretches illustrate the sensitive detection scheme of this cryogenic tagging spectroscopy approach.

Tyramine

The very large dipole for N-protonated PABA (i.e., 13D) accounts for the stronger PABA●ACN binding energy, which may not be completely representative of ACN-tagging spectroscopy of other analytes. The molecular system tyramine and its proposed CID product ion structures are depicted in Figure 4A. The spirocyclopropane structure for the ammonia loss *m/z* 121 product can be rationalized by a nucleophilic attack from the aromatic ring, meaning that the positive charge is delocalized over the aromatic ring. Similar structures were suggested in the fragmentation chemistry of protonated tryptophan,[34] which were later confirmed based on IRMPD spectra.[35]

The raw ESI mass spectrum in Figure 4B shows the presence of tyramine, its CID product ions, and their corresponding tagged complexes. The apparent tagging efficiencies are shown to vary quite considerably between different analyte ions, as summarized in Table 2. The

observation of tagged CID product ions would seem to support the thesis that those tagged complexes are formed by gas-phase attachment after nozzle-skimmer dissociation. As will be shown below, this hypothesis is not correct. Figure 4C illustrates how four discrete tagged species can be mass selected in the same experiment. As the precursor and photofragment mass channels are all independent of each other, irradiation of this mixture would in principle allow recording of the IRPD spectra of all four tagged ions in parallel in a multiplexed approach.

Figure 5 shows the IRPD spectra of tyramine●ACN (A) and *m/z*121●ACN (C), as well as the IRMPD spectrum for tyramine (B) for comparison. Note that the IRPD spectra for *m/z*103●ACN and *m/z*91●ACN_2 did not yield any detectable IR photodissociation (not shown). This indicates that those molecular ions are strongly bound to the ACN molecules, possibly forming a covalent complex. Such a hypothesis would also rationalize the unusually high apparent tagging efficiencies for *m/z*103●ACN and *m/z*91●ACN_2 in Table 2.

A number of modes can be distinguished in Figure 5, including the phenol OH stretch, as well as various NH and CH stretches. The band assignments and positions are summarized in Table 3. The band positions for *m/z*121●ACN are not compatible with a con-covalent complex. The phenol OH stretch is only very slightly redshifted for *m/z*121●ACN compared to tyramine●ACN. This is unexpected, as the ACN in *m/z*121●ACN would almost certainly have to bind to the phenol OH, in the process significantly redshifting the phenol OH stretch. Tentatively, a covalent structure is proposed for *m/z*121●ACN, which will be further characterized in an upcoming study.

The comparisons between the tyramine●ACN IRPD and tyramine IRMPD spectra are again telling, as modes are sometimes redshifted substantially in the IRMPD spectra (e.g. 65 cm^{-1} for aromatic CH stretches), but sometimes only marginally redshifted (e.g. 4 cm^{-1} for phenol OH stretch). This once again underlines the dynamic nature of redshifting in IRMPD due to anharmonic effects.

Conclusions

In this proof-of-principle experiment, we have shown that infrared ion spectroscopy on tagged ions can be carried out inside a mass-selective cryogenic 2D linear ion trap. This approach presents a number of advantages in terms of carrying out infrared photodissociation experiments:

- The instrument is compact, requiring no mass analyzer after the cryogenic trap.
- Tagging efficiency is found to be relatively high for singly ACN-tagged ions, which minimizes ion signal dilution, and thus maximizes sensitivity.
- Several tagged ions can be mass isolated together, thus allowing a multiplexed approach, where the IR spectra of multiple tagged analyte ions are recorded in parallel. This increases the duty cycle of infrared ion spectroscopy, where normally only one analyte ion is probed at one wavelength at any one time.

- Photodissociation efficiency is high even at lower pulse energies, which suggests a good overlap between the OPO/A beam and the ion cloud.

As has been shown in many studies, cryogenic temperatures are essential in order to achieve higher spectral resolution. In future studies, we will demonstrate the effect of the trap temperature on how well bands can be separated. Operating a 2D linear ion trap at cryogenic temperatures does not diminish its performance as a mass spectrometer, even if the trap does need to be warmed up periodically to prevent icing, and thus build-up of charges. OPO/A's remain the state-of-the-art technology for tunable IR output from 2000–4000 cm^{-1}. By use of down-conversion crystals, the important fingerprint region (800–2000 cm^{-1}) can also be accessed. The sensitivity limit of a 2D linear ion trap is excellent, making it in principle a powerful tool in IR action spectroscopy; the lower concentrations studied here (i.e., 10^{-7}M) are certainly biologically relevant. The key improvement in terms of sample consumption now lies in a faster duty of the experiment, ideally matching the 10 Hz of the OPO/A. The greatest potential for cryogenic infrared ion spectroscopy is probably in the realm of small molecule identification, as discussed in some detail in a critical insight article.[1]

It remains to be seen how useful solvent tagging would be in terms of identifying unknown analytes. The interactions of the solvent with the analyte can shift vibrational modes, and the solvent has IR-active modes of its own that may obfuscate interpretation. For the analytes and tag considered here, the binding energies likely exceed a single photon, thus making the IRPD yield non-linear with power. Tagging with more weakly-bound atoms or molecules, which additionally have no or fewer IR-active modes, would overcome this problem. Preliminary experiments have shown that in-trap N_2-tagging is possible, but challenges remain to make the ion signal more stable. A constraint in the current design is the rather lengthy pump-down delay, which does not make use of the 10 Hz repetition rate of the OPO/A. Improved designs for pulsed gas injection could address this issue. Despite these challenges, the development of a mass-selective cryogenic linear ion trap is an important first step for making cryogenic infrared ion spectroscopy a more routine bioanalytical tool for low-abundance biological samples.

The project was financially supported by the United States National Science Foundation (NSF) under grant number CHE-1403262 and the United States National Institutes of Health (NIH) under grant number R01GM110077. Todd Prox and Brian Smith in our machine shop are gratefully acknowledged for constructing the *cryo*LIT and a number of custom parts of our set-up. Stanley Psych and David Murzynski in our electronics shop are acknowledged for their help with electronics circuits. Dr. Philip Remes and Dr. Jae Schwartz from Thermo-Fisher are thanked for providing a Thermo rf power supply to enable these experiments.

Supplementary Material

Refer to Web version on PubMed Central for supplementary material.

Publications

1. Cismesia AP, Bailey LS, Bell MR, Tesler LF, Polfer NC. Making Mass Spectrometry See the Light: The Promises and Challenges of Cryogenic Infrared Ion Spectroscopy as a Bioanalytical Technique. Journal of the American Society for Mass Spectrometry. 2016; 27:757–766. [PubMed: 26975370]

2. Oomens J, Sartakov BG, Meijer G, von Helden G. Gas-phase infrared multiple photon dissociation spectroscopy of mass-selected molecular ions. International Journal of Mass Spectrometry. 2006; 254:1–19.

3. Polfer NC. Infrared multiple photon dissociation spectroscopy of trapped ions. Chemical Society Reviews, The Royal Society of Chemistry. 2011; 40:2211–2221.

4. Oepts D, van der Meer AFG, van Amersfoort PW. The Free-Electron-Laser user facility FELIX. Infrared Physics & Technology. 1995; 36:297–308.

5. Lemaire, J., Boissel, P., Heninger, M., Mauclaire, G., Bellec, G., Mestdagh, H., Simon, A., Caer, SL., Ortega, JM., Glotin, F., Maitre, P. Physical Review Letters. Vol. 89. American Physical Society; 2002. Gas Phase Infrared Spectroscopy of Selectively Prepared Ions; p. 273002

6. Schöllkopf W, Gewinner S, Junkes H, Paarmann A, von Helden G, Bluem H, Todd AMM. The new IR and THz FEL facility at the Fritz Haber Institute in Berlin. 2015; 9512 95121L-95121L-13.

7. Okumura M, Yeh LI, Myers JD, Lee YT. Infrared spectra of the cluster ions H7O+3-H2 and H9O +4-H2. The Journal of Chemical Physics. 1986; 85:2328–2329.

8. Kamrath MZ, Relph RA, Guasco TL, Leavitt CM, Johnson MA. Vibrational predissociation spectroscopy of the H2-tagged mono- and dicarboxylate anions of dodecanedioic acid. International Journal of Mass Spectrometry. 2011; 300:91–98.

9. Thompson MC, Ramsay J, Weber JM. Solvent-Driven Reductive Activation of CO2 by Bismuth: Switching from Metalloformate Complexes to Oxalate Products. Angewandte Chemie International Edition. 2016; 55:15171–15174. [PubMed: 27730755]

10. Duffy EM, Marsh BM, Voss JM, Garand E. Characterization of the Oxygen Binding Motif in a Ruthenium Water Oxidation Catalyst by Vibrational Spectroscopy. Angewandte Chemie International Edition. 2016; 55:4079–4082. [PubMed: 26890565]

11. Masson A, Kamrath MZ, Perez MAS, Glover MS, Rothlisberger U, Clemmer DE, Rizzo TR. Infrared Spectroscopy of Mobility-Selected H+-Gly-Pro-Gly-Gly (GPGG). Journal of the American Society for Mass Spectrometry. 2015; 26:1444–1454. [PubMed: 26091889]

12. Goebbert DJ, Wende T, Bergmann R, Meijer G, Asmis KR. Messenger-Tagging Electrosprayed Ions: Vibrational Spectroscopy of Suberate Dianions. The Journal of Physical Chemistry A, American Chemical Society. 2009; 113:5874–5880.

13. Jašík J, Roithová J. Infrared spectroscopy of CHCl2+ molecular dications. International Journal of Mass Spectrometry. 2015; 377:109–115.

14. Power B, Haldys V, Salpin J-Y, Fridgen TD. Structures of [M(Ura-H)(H2O)n]+ (M = Mg, Ca, Sr, Ba; n = 1–3) complexes in the gas phase by IRMPD spectroscopy and theoretical studies. Journal of Mass Spectrometry. 2016; 51:236–244. [PubMed: 26956390]

15. Chang TM, Prell JS, Warrick ER, Williams ER. Where's the Charge? Protonation Sites in Gaseous Ions Change with Hydration. Journal of the American Chemical Society, American Chemical Society. 2012; 134:15805–15813.

16. Ishiuchi, S-i, Wako, H., Kato, D., Fujii, M. High-cooling-efficiency cryogenic quadrupole ion trap and UV-UV hole burning spectroscopy of protonated tyrosine. Journal of Molecular Spectroscopy. 2017; 332:45–51.

17. Burke NL, Redwine JG, Dean JC, McLuckey SA, Zwier TS. UV and IR spectroscopy of cold protonated leucine enkephalin. International Journal of Mass Spectrometry. 2015; 378:196–205.

18. Mohrbach J, Lang J, Dillinger S, Prosenc M, Braunstein P, Niedner-Schatteburg G. Vibrational fingerprints of a tetranuclear cobalt carbonyl cluster within a cryo tandem ion trap. Journal of Molecular Spectroscopy. 2017; 332:103–108.

19. Heine N, Asmis KR. Cryogenic ion trap vibrational spectroscopy of hydrogen-bonded clusters relevant to atmospheric chemistry. International Reviews in Physical Chemistry, Taylor & Francis. 2015; 34:1–34.

20. Günther A, Nieto P, Müller D, Sheldrick A, Gerlich D, Dopfer O. BerlinTrap: A new cryogenic 22-pole ion trap spectrometer. Journal of Molecular Spectroscopy. 2017; 332:8–15.

21. Fanghänel S, Asvany O, Schlemmer S. Optimization of RF multipole ion trap geometries. Journal of Molecular Spectroscopy. 2017; 332:124–133.

22. Chang TM, Chakrabarty S, Williams ER. Hydration of Gaseous m-Aminobenzoic Acid: Ionic vs Neutral Hydrogen Bonding and Water Bridges. Journal of the American Chemical Society, American Chemical Society. 2014; 136:10440–10449.

23. Gulyuz K, Stedwell CN, Wang D, Polfer NC. Hybrid quadrupole mass filter/quadrupole ion trap/time-of-flight-mass spectrometer for infrared multiple photon dissociation spectroscopy of mass-selected ions. Review of Scientific Instruments. 2011; 82:054101. [PubMed: 21639521]

24. Patrick AL, Cismesia AP, Tesler LF, Polfer NC. Effects of ESI conditions on kinetic trapping of the solution-phase protonation isomer of p-aminobenzoic acid in the gas phase. International Journal of Mass Spectrometry. 2016 Vol. submitted.

25. Ouyang Z, Wu G, Song Y, Li H, Plass WR, Cooks RG. Rectilinear Ion Trap: Concepts, Calculations, and Analytical Performance of a New Mass Analyzer. Analytical Chemistry, American Chemical Society. 2004; 76:4595–4605.

26. Wang, L., Xu, F., Dai, X., Fang, X., Ding, CF. Journal of the American Society for Mass Spectrometry. Vol. 25. Springer US; 2014. Development and Investigation of a Mesh-Electrode Linear Ion Trap (ME-LIT) Mass Analyzer; p. 548-555.

27. Guan S, Marshall AG. Stored waveform inverse Fourier transform axial excitation/ejection for quadrupole ion trap mass spectrometry. Analytical Chemistry, American Chemical Society. 1993; 65:1288–1294.

28. Cismesia AP, Bell MR, Tesler LF, Bailey LS, Polfer NC. A Mass-selective Cryogenic 2D Linear Ion Trap for Infrared Ion Spectroscopy. in preparation.

29. Bosenberg WR, Guyer DR. Broadly tunable, single-frequency optical parametric frequency-conversion system. Journal of the Optical Society of America B, OSA. 1993; 10:1716–1722.

30. Schmidt, J., Meyer, MM., Spector, I., Kass, SR. The Journal of Physical Chemistry A. Vol. 115. American Chemical Society; 2011. Infrared Multiphoton Dissociation Spectroscopy Study of Protonated p-Aminobenzoic Acid: Does Electrospray Ionization Afford the Amino- or Carboxy-Protonated Ion? In; p. 7625-7632.

31. Campbell JL, Le Blanc JCY, Schneider BB. Probing Electrospray Ionization Dynamics Using Differential Mobility Spectrometry: The Curious Case of 4-Aminobenzoic Acid. Analytical Chemistry, American Chemical Society. 2012; 84:7857–7864.

32. Seo, J., Warnke, S., Gewinner, S., Schollkopf, W., Bowers, MT., Pagel, K., von Helden, G. Physical Chemistry Chemical Physics. Vol. 18. The Royal Society of Chemistry; 2016. The impact of environment and resonance effects on the site of protonation of aminobenzoic acid derivatives; p. 25474-25482.

33. Linstrom, PJ., Mallard, WG., editors. NIST Chemistry WebBook. NIST Standard Reference Database Number 69. National Institute of Standards and Technology; Gaithersburg MD: p. 20899(retrieved May 22, 2017)

34. Lioe H, O'Hair RAJ, Reid GE. Gas-phase reactions of protonated tryptophan. Journal of the American Society for Mass Spectrometry. 2004; 15:65–76. [PubMed: 14698557]

35. Mino, WK., Gulyuz, K., Wang, D., Stedwell, CN., Polfer, NC. The Journal of Physical Chemistry Letters. Vol. 2. American Chemical Society; 2011. Gas-Phase Structure and Dissociation Chemistry of Protonated Tryptophan Elucidated by Infrared Multiple-Photon Dissociation Spectroscopy; p. 299-304.

36. Lanucara, F., Chiavarino, B., Scuderi, D., Maitre, P., Fornarini, S., Crestoni, ME. Chemical Communications. Vol. 50. The Royal Society of Chemistry; 2014. Kinetic control in the CID-induced elimination of H3PO4 from phosphorylated serine probed using IRMPD spectroscopy; p. 3845-3848.

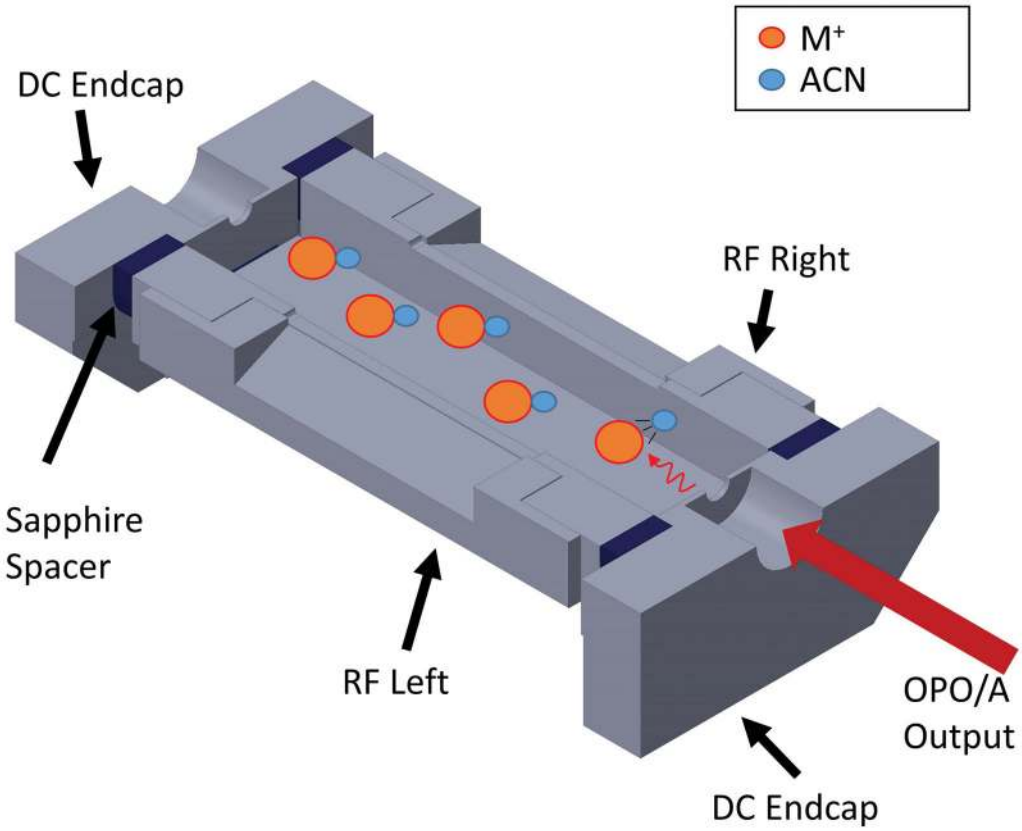

Figure 1.

Isometric sectional view of cryogenic 2D linear ion trap (cryoLIT). DC endcap electrodes, RF electrodes and sapphire spacers are indicated. Resonant photon absorption from IR light source leads to photodissociation of tagged analyte M^+●ACN ions.

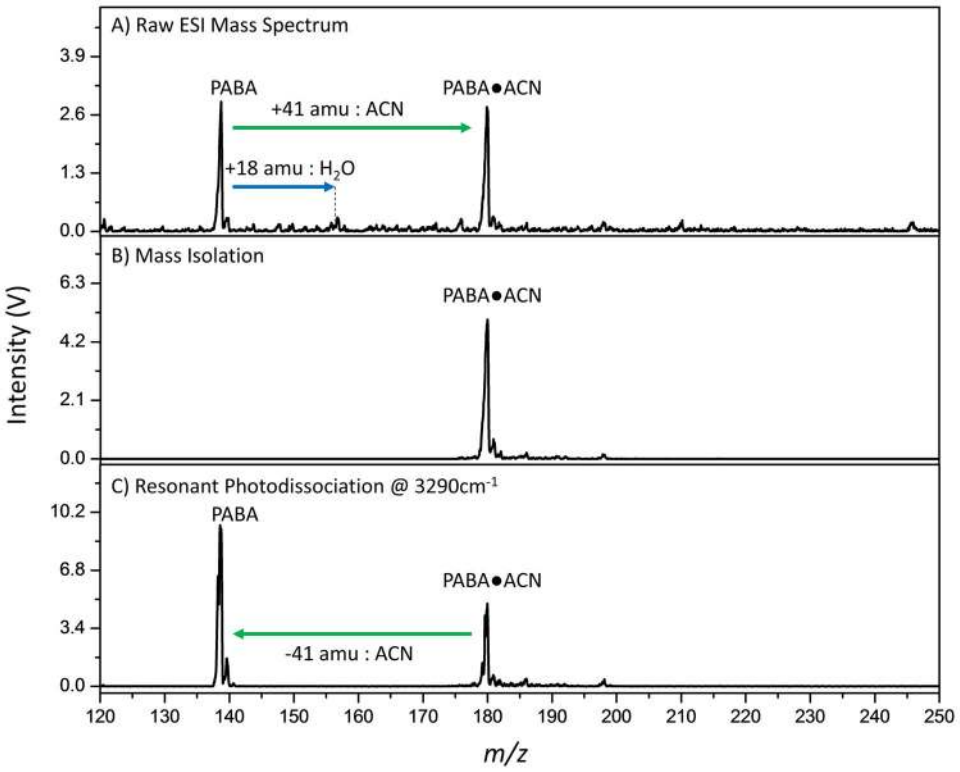

Figure 2.

Mass spectra of (A) electrosprayed PABA solution trapped and detected in *cryoLIT*, (B) SWIFT isolation of tagged ion PABA●ACN, (C) resonant photodissociation of PABA●ACN to PABA.

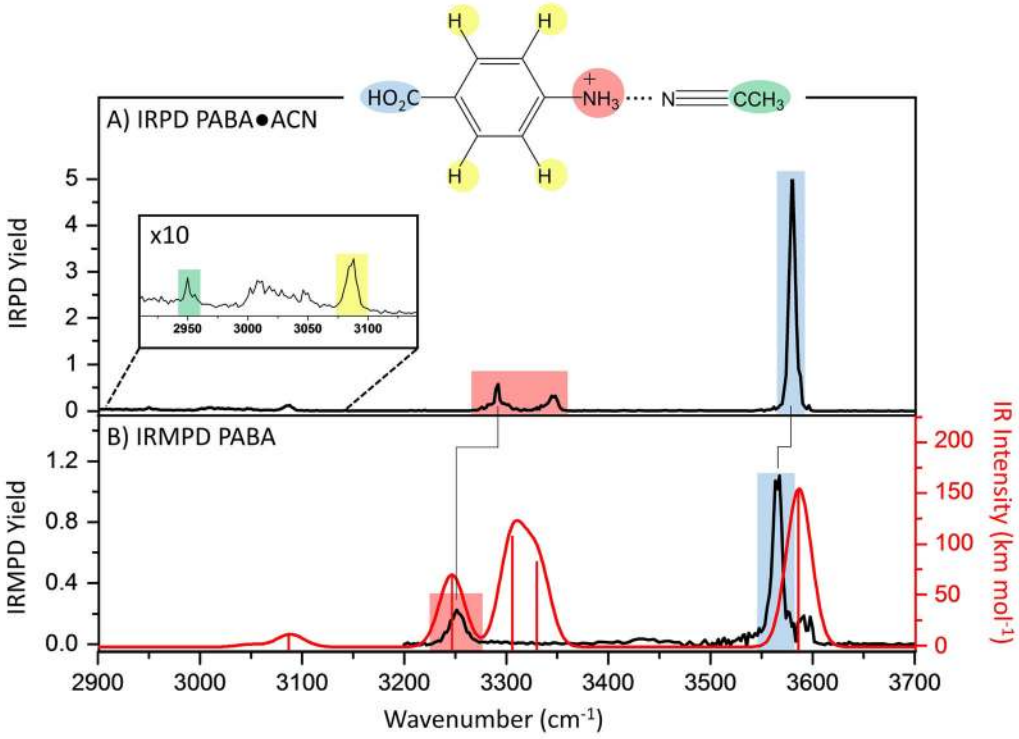

Figure 3.

(A) Cryogenic IRPD spectrum of protonated PABA●ACN. (B) Room-temperature IRMPD spectrum protonated PABA (in black) compared to computed IR absorption spectrum (B3LYP/cc-PVTZ) of untagged PABA (in red). Band assignments indicated by color-coding.

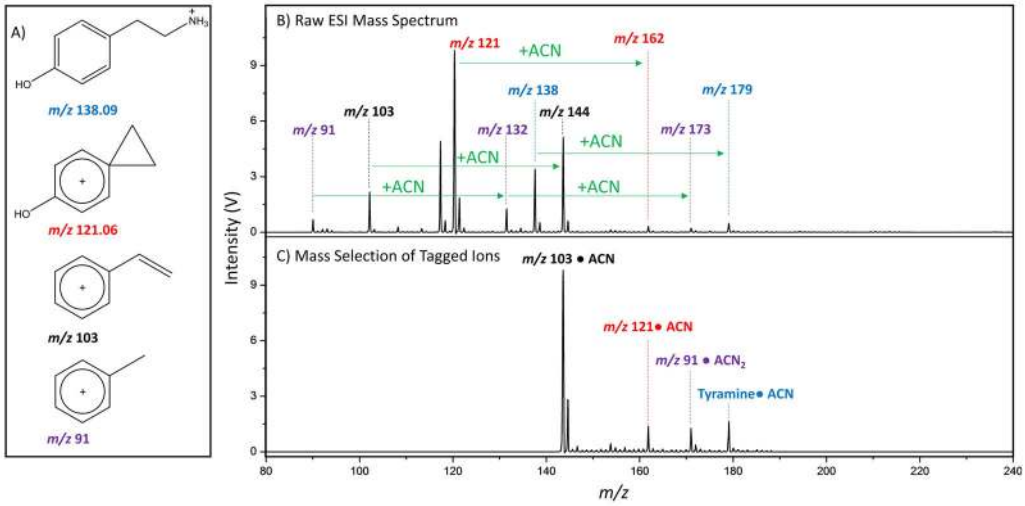

Figure 4.

(A) Proposed structures for protonated tyramine (*m/z* 138) and various CID products. Mass spectra of (B) electrosprayed tyramine solution trapped and detected in *cryoLIT*, (C) SWIFT isolation of tagged ions at *m/z* 144 (*m/z*103●ACN), 162 (*m/z*121●ACN), 173 (*m/z*91●ACN_2), and 179 (*m/z*138●ACN=tyramine●ACN).

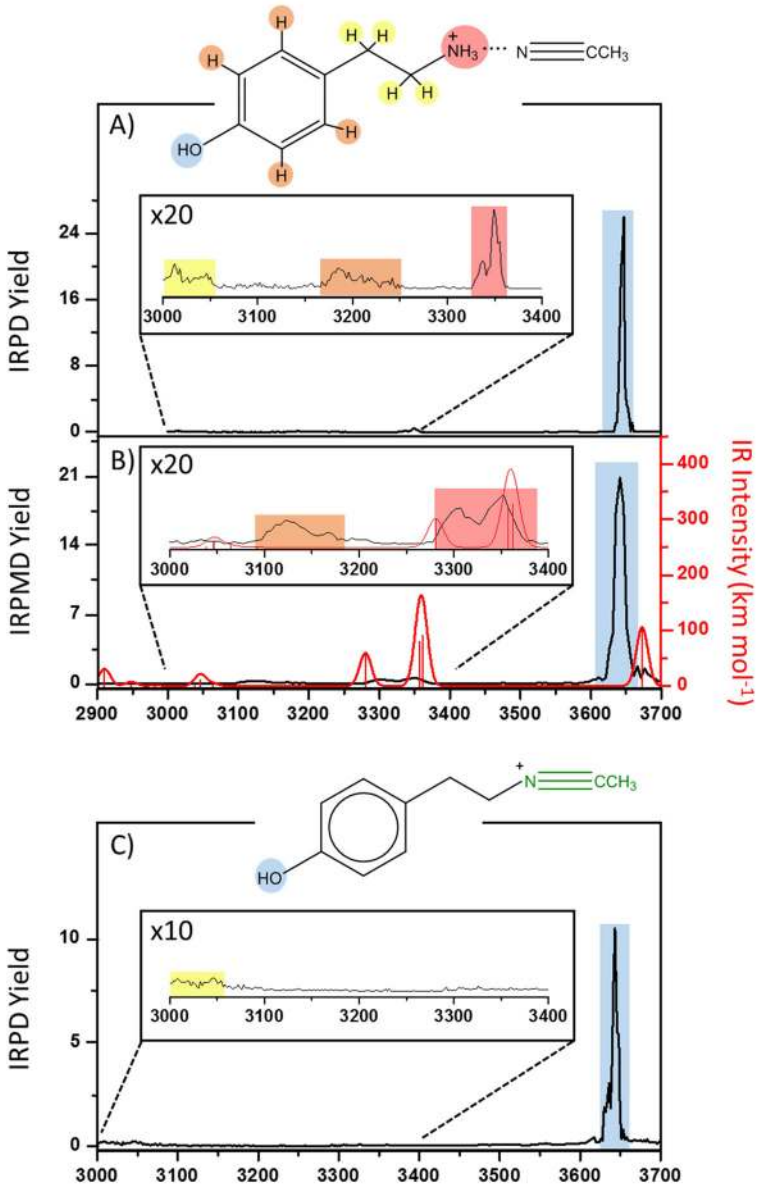

Figure 5.

Comparison of (A) IRPD spectrum of tyramine●ACN, and (B) IRMPD spectrum of tyramine (in black) and DFT computed spectrum (in red). (C) IRPD spectrum of tagged *m/z* 121 fragment, *m/z*121●ACN, for which a covalently-tagged structure is proposed.

Table 1

Experimental IRMPD and IRPD band positions for PABA compared to computed band positions.

Vibrational Modes	Band Positions/cm^{-1} B3LYP/cc-PVTZ (scaling factor 0.960)[36]	Band Positions/cm^{-1} (FWHM) IRMPD Experimental	Band Positions/cm^{-1} (FWHM) IRPD Experimental
OH Stretch	3586	3565 (11)	3580 (7.5)
NH_3^+ Stretches	3330, 3306, 3247	3250 (18)	3345 (7.5) 3291 (8.5)
CH Stretch	3087	-	3088 (32.5)
ACN Stretch	N/A	N/A	2950 (3.5)

Table 2

Tagging efficiency for tagged analytes in Figure 4

Tagged Ion Mass	Assignment	Tagging Efficiency
m/z 132	*m/z* 91●ACN	60.5%
m/z 144	*m/z* 103●ACN	74.7%
m/z 162	*m/z* 121●ACN	2.6%
m/z 173	*m/z* 91●ACN_2	11.9%
m/z 179	tyramine●ACN	12.6%

Table 3

Experimental IRPD band positions for tyramine●ACN and *m/z*121●ACN CID product ion compared to IRMPD results and computed band positions for tyramine.

Vibrational Modes	Band Positions/cm^{-1} B3LYP/cc-PVTZ (scaling factor 0.960)[36]	Band Positions/cm^{-1} (FWHM) IRMPD Experimental	Band Positions/cm^{-1} (FWHM) IRPD Experimental (m/z 138)	Band Positions/cm^{-1} (FWHM) IRPD Experimental (m/z 121)
OH Stretch	3673.8	3642 (15)	3646 (7)	3643 (7.5)
NH_3^+ Stretches	3362.2 3357.65 3280.9	3347 (27.5) 3307 (35.5)	3351(9) 3338(12)	-
Aromatic CH Stretches	3092.3 3064.3 3046.8 3046.2	3122 (42)	3187 (19)	-
Aliphatic CH Stretches	3038.4 2982.5 2982.5 2948.5 2910.5	-	3046 (6.0) 3012 (8.5)	3046 (6.0) 3007 (4.5)